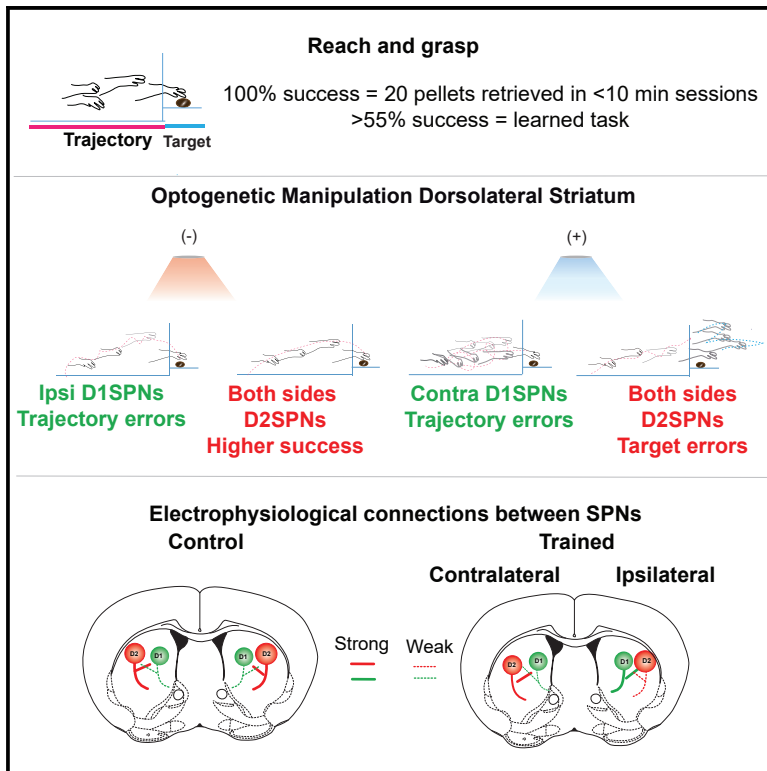# Cell Reports

Striatal bilateral control of skilled forelimb movement

Graphical Abstract

Authors

Violeta G. Lopez-Huerta, Jai A. Denton, Yoko Nakano, Omar Jaidar, Marianela Garcia-Munoz, Gordon W. Arbuthnott

Correspondence

violeta@ifc.unam.mx (V.G.L.-H.), gordon@oist.jp (G.W.A.)

In Brief

Lopez-Huerta et al. motivate mice to use their preferred paw to reach and grasp. Optogenetic manipulation of striatal D1 output neurons induces trajectory errors and D2 inhibition improves whereas activation disrupts target success. Performance modifies connectivity bilaterally among striatal output neurons recorded *ex vivo*.

Highlights

- Ipsilateral and contralateral striatal outputs control skilled forepaw movement

- Direct and indirect striatal projection neurons differentially affect skilled movements

- D1SPN projections control trajectory, whereas D2SPNs influence the target

- Performance of learned skilled movements modifies striatal synaptic connectivity

CellPress

Cell Reports

Article

Striatal bilateral control of skilled forelimb movement

Violeta G. Lopez-Huerta,[1,2,3,*] Jai A. Denton,[1,4] Yoko Nakano,[1] Omar Jaidar,[1,5] Marianela Garcia-Munoz,[1] and Gordon W. Arbuthnott[1,6,*]

[1]Brain Mechanisms for Behaviour Unit, Okinawa Institute of Science and Technology Graduate University, Onna-son, Okinawa 904-0495, Japan
[2]Stanley Center for Psychiatric Research, Broad Institute of MIT and Harvard, Cambridge, MA 02142, USA
[3]Institute of Cellular Physiology, National University of Mexico, Mexico City 04510, Mexico
[4]Institute of Vector-Borne Disease, Monash University, Clayton, VIC 3800, Australia
[5]Chem-H-/Neuro Research Building, Neurosurgery School of Medicine, Stanford University, Stanford, CA 94305, USA
[6]Lead contact
*Correspondence: violeta@ifc.unam.mx (V.G.L.-H.), gordon@oist.jp (G.W.A.)
https://doi.org/10.1016/j.celrep.2020.108651

SUMMARY

Skilled motor behavior requires bihemispheric coordination, and participation of striatal outputs originating from two neuronal groups identified by distinctive expression of D1 or D2 dopamine receptors. We trained mice to reach for and grasp a single food pellet and determined how the output pathways differently affected forelimb trajectory and task efficiency. We found that inhibition and excitation of D1-expressing spiny projection neurons (D1SPNs) have a similar effect on kinematics results, as if excitation and inhibition disrupt the whole ensemble dynamics and not exclusively one kind of output. In contrast, D2SPNs participate in control of target accuracy. Further, *ex vivo* electrophysiological comparison of naive mice and mice exposed to the task showed stronger striatal neuronal connectivity for ipsilateral D1 and contralateral D2 neurons in relation to the paw used. In summary, while the output pathways work together to smoothly execute skill movements, practice of the movement itself changes synaptic patterns.

INTRODUCTION

A simple daily task, like grasping a cup of coffee, requires a combination of fine movements leading to a goal-directed action (d'Avella et al., 2003; Graybiel, 2008; Overduin et al., 2012; Wymbs and Grafton, 2015). Acquisition and performance of these skilled movements are known to involve bilateral control of motor programs in different brain areas (Brus-Ramer et al., 2009; Donchin et al., 1998; Li et al., 2016; Tecuapetla et al., 2014; Vaidya et al., 2015; van den Berg et al., 2011; Verstynen et al., 2005). Participation of both hemispheres is known for the cortex, especially when high dexterity is involved (Davare et al., 2007; Ganguly et al., 2009; van den Berg et al., 2011). However, the precise role of ipsilateral and contralateral basal ganglia nuclei is not yet understood.

The striatum participates in selection and performance of motor sequences (Kravitz et al., 2010; Li et al., 2016; Yin et al., 2009a; Yin and Knowlton, 2006), including skilled forelimb tasks like reaching and grasping (Lopez-Huerta et al., 2016; MacLellan et al., 2006; Miklyaeva et al., 1994; Whishaw et al., 2007). Balanced activation of striatal spiny projection neurons (SPNs) helps to smoothly implement motor repertoires, enabling skilled movement performance (Graybiel, 2008; Lopez-Huerta et al., 2016; Tecuapetla et al., 2014; Yin et al., 2009a). SPNs are recruited in behavior as a link between cortical activation and movement via recurrent striato-nigro-thalamo-cortical routes and via the brainstem motor "centers." In addition to their final targets, SPNs also connect locally via extensive axon collaterals that inhibit neighboring neurons (López-Huerta et al., 2013; Taverna et al., 2004; Tepper et al., 2008). Connections between D1 and D2 receptor-expressing SPNs are thought to regulate intrastriatal information processing units that govern the final basal ganglion output (Tepper et al., 2008; Wilson, 2007).

In this study, we used selective optogenetic manipulation of striatal output neurons during performance of a unimanual skilled motor task. Our experiments show clear changes in behavior following optogenetic manipulation of each group of SPNs, but those changes cannot be explained entirely by the optogenetically evoked activity. For example, light-induced stimulation or inhibition of D1-expressing SPNs (D1SPNs) produces similar actions on movements, which compels consideration of circuit interactions. Because acquisition and consolidation of a motor task produce dynamic modifications in striatal neuronal activity related to synaptic contact reorganization (Hawes et al., 2015; Yin et al., 2009a), we also studied, *ex vivo*, electrophysiological reciprocal interactions between the two classes of SPNs and found that the behavioral experience can indeed produce a dynamic change in striatal circuit interaction and network activity.
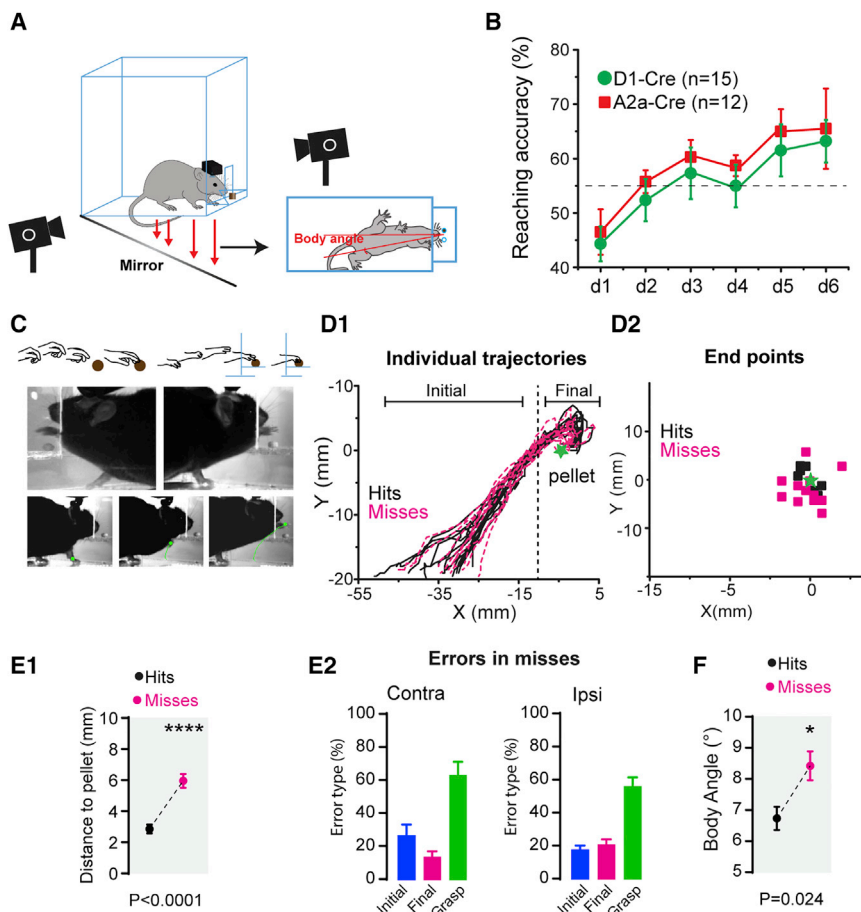
Figure 1. Reaching behavior in control mice

(A) Sketch of the training paradigm. Two high-speed cameras follow the reach in two dimensions, whereas a third collects the position of the animal from the mirror under the chamber. Postural measurements of body angle with respect to the chamber wall were collected by this camera. Animals were free to choose their preferred paw, and recording or stimulation sides always referred to the side of the preferred paw.

(B) Development of reaching success over 6 days of training. There was no difference between the two groups of transgenic animals. Data are plotted as mean ± SEM.

(C) Photographs from the side of the chamber. The sketches above indicate the progress of a reach. Cameras allow tracking of either paw.

(D1) Individual trajectories of the paw during hit and missed trials.

(D2) Paw endpoints in relation to the pellet.

(E1) Summary of endpoint distance from the target in hits = 3.16, misses = 6.08 mm (Mann-Whitney-Wilcoxon test miss versus hit U = 4,184, p < 0.0001, n_{hits} = 123, n_{misses} = 129 from 28 mice).

(E2) Proportions of the three kinds of errors made by mice (see also Table 1). All three occur with equal probability regardless of whether the contralateral or ipsilateral paw was used (n_{ipsi} = 67, n_{contra} = 59 from 28 mice), but the proportions change in the optogenetic experiments below (Figures 2 and 3).

(F) Differences in body angle in the two kinds of trials. Hits 6.7° ± 4°, misses = 8.4° ± 5.3° (Mann-Whitney-Wilcoxon test U = 6,437, p = 0.0243, n_{hits} = 118, n_{misses} = 133 from 28 mice).

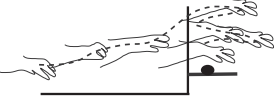See also Figure S1.

RESULTS

Reaching behavior

To dissect the participation of contralateral and ipsilateral SPN populations during unilateral forelimb skilled movement, we used D1-Cre (D1) and A2a-Cre (D2) mice. First, they were prepared surgically for optogenetic manipulations. After a recovery period, the animals were trained for 6–10 days in a single-pellet reach-to-grasp task. The training chamber had an opening through which mice could reach with only one forelimb to grasp a food pellet (Figure 1A). Results are presented for the ipsilateral or contralateral hemisphere prepared for optical manipulation in relation to the preferred paw (STAR methods: Single-pellet, reach-to-grasp task). Animals that achieved more than 55% success at retrieving pellets (scored as pellets obtained by grasping divided by the total number of reaches) were used in further experiments (Figure 1B). Trained mice exhibited a stereotypical reaching trajectory shown by high-speed videography. This allowed us to study the kinematics of different stages of the skilled movement (Figures 1C and 1D1). Considering that mice, even after several days of training, sometimes failed to grasp the pellet, we further analyzed differences between hit and missed trials under control conditions. During missed events, the paw started a grasping movement farther away from the pellet (endpoint)

compared with hit events (Figures 1D2 and 1E1). Further observation led us to conclude that the lack of success to obtain the pellet resulted from three different types of errors that we called initial, final, and grasp. In the initial error, the mouse changed trajectory before the paw crossed the opening of the chamber. In the final error, the animal changed trajectory after the paw crossed the opening (Figure 1E2), and the grasp error consisted of failure to collect the pellet. By far the most common under control conditions was the grasp error, occurring in more than half of the misses (contralateral [contra], 62.3%; ipsilateral [ipsi], 57.6%). The initial errors (contra, 26.3%; ipsi, 13.6%) and final errors (contra, 20.9%; ipsi, 17.9%) were less common (Figure 1E2; Table 1). Finally, misses were also associated with a difference in the body angle related to the animals' posture (Figure 1F). These results show that even this simple task contains several motor components that allow fluid execution of movement to attain a goal.

Optical manipulations change movement kinematics

In D1-Cre and A2a-Cre mice, we enabled selective expression of ChR-2-mCherry (for activation) or Halo-R-YFP (for inhibition) by viral injection of Cre-dependent adeno-associated virus (AAV) serotype 1 into the dorsolateral striatum (Figures 2A, 2C, 3A, 3C, and S1). Additionally, we implanted a cannula and an optical

Table 1. Details of behavioral analyses

Retrieval success optogenetic activation ipsilateral D1SPNs	Retrieval success optogenetic Activation contralateral D1SPNs	Retrieval success optogenetic Activation ipsilateral D2SPNs	Retrieval success optogenetic activation contralateral D2SPNs
% control, t test, p =	% control, t test, p =	% control, t test, p =	% control, t test, p =
120.7 ± 23.6, t = 0.92, p = 0.35	56.6 ± 7.6, t = −3.6, p = 0.0028	64.9 ± 8.8, t = 4.2, p = 0.00013	37.1 ± 14.6, t = 4.9, p = 0.00021
Retrieval success optogenetic inhibition ipsilateral D1SPNs	retrieval success optogenetic inhibition contralateral D1SPNs	Retrieval success optogenetic inhibition ipsilateral D2SPNs	Retrieval success optogenetic inhibition contralateral D2SPNs
% control, t test, p =	% control, t test, p =	% control, t test, p =	% control, t test, p =
50.7 ± 12.7, t = 4.47, p = 0.00052	163 ± 38.8, t = −2.8, p = 0.013	102.1 ± 21.3, t = 1.39, p = 0.17	160.7 ± 19.2, t = −2.6, p = 0.01
I	initial trajectory error	changes in initial trajectory; i.e., before the paw crossed the opening of the chamber	
II	final trajectory error	changes in the final trajectory; i.e., after paw crossed the chamber opening	
III	grasp failure	animals reach correctly, start the grasping motion, but fail the grasp by hitting (a) or dropping the pellet (b).	
Trajectory dispersion (kinematics)-PCA optogenetic activation ipsilateral D1SPNs	Trajectory dispersion (kinematics)-PCA optogenetic activation contralateral D1SPNs	Trajectory dispersion (kinematics)-PCA optogenetic activation ipsilateral D2SPNs	Trajectory dispersion (kinematics)-PCA optogenetic activation contralateral D2SPNs
Trajectory overlap	Trajectory overlap	Trajectory overlap	Trajectory overlap
hits = 39.7 ± 24.2, fails = 25.7 ± 6.9<	hits = 39.7 ± 24.2, fails = 25.7 ± 6.9	hits = 39.7 ± 24.2, fails = 25.7 ± 6.9	hits = 39.7 ± 24.2, fails = 25.7 ± 6.9
Trajectory dispersion (kinematics)-PCAoptogenetic inhibition ipsilateral D1SPNs	Trajectory dispersion (kinematics)-PCAoptogenetic inhibition contralateral D1SPNs	Trajectory dispersion (kinematics)-PCAoptogenetic inhibition ipsilateral D2SPNs	Trajectory dispersion (Kinematics)-PCAoptogenetic inhibition contralateral D2SPNs
Trajectory overlap	Trajectory overlap	Trajectory overlap	Trajectory overlap
hits = 30 ± 20, fails = 44.5 ± 26.5<	hits = 62 ± 3, fails = 17 ± 4	hits = 65 ± 3, fails = 50 ± 20	hits = 74.5 ± 8.5, fails = 47 ± 25<

Retrieval success (Figures 2 and 3) results from comparisons between mice in trials before and during optogenetic manipulation (STAR methods: Kinematic quantification of reaching). In non-stimulation trials, errors were distributed similarly regardless of whether the preferred paw was ipsilateral or contralateral to the operated hemisphere. Activation in particular caused errors (I, initial; II, final trajectory; and/or III, grasp) that resulted in significant changes in retrieval success. Inhibition of D2SPNs increased retrieval success, and ipsilateral inhibition of D1SPNs was associated with longer and more variable trajectories.

fiber attached to an infrared receiver to allow wireless optogenetic manipulation (Videos S1, S2, and S3). At the beginning of the skilled movement, photostimulation was delivered continuously until a hit or a miss occurred (1.5 s on average). As described in STAR methods: AAV expression and stereotaxic surgery, task performance was compared before and after optogenetic stimulation in individual mice.

Optogenetic activation
We studied the effects of SPN activation in contralateral or ipsilateral hemispheres according to the preferred paw (Table 1).

Contralateral activation of D1SPNs decreased retrieval success to 64.9% ± 8.8% compared with control values before activation (Figure 2B1). Trajectory tracking showed a drastic change in the initial reaching trajectory with an increase in initial error type I (Figure 2B2). A quantitative comparison of the different trajectories was obtained with principal-component analysis (PCA) followed by k-means clustering (Figure S2). Trajectories from missed and hit trials during D1SPN activation separated in a cluster with almost no overlap with the control cluster, indicating low similarity (Figures S2B and S3B). Interestingly, activation of contralateral D2SPNs also reduced retrieval success to 37.1% ± 14.6%
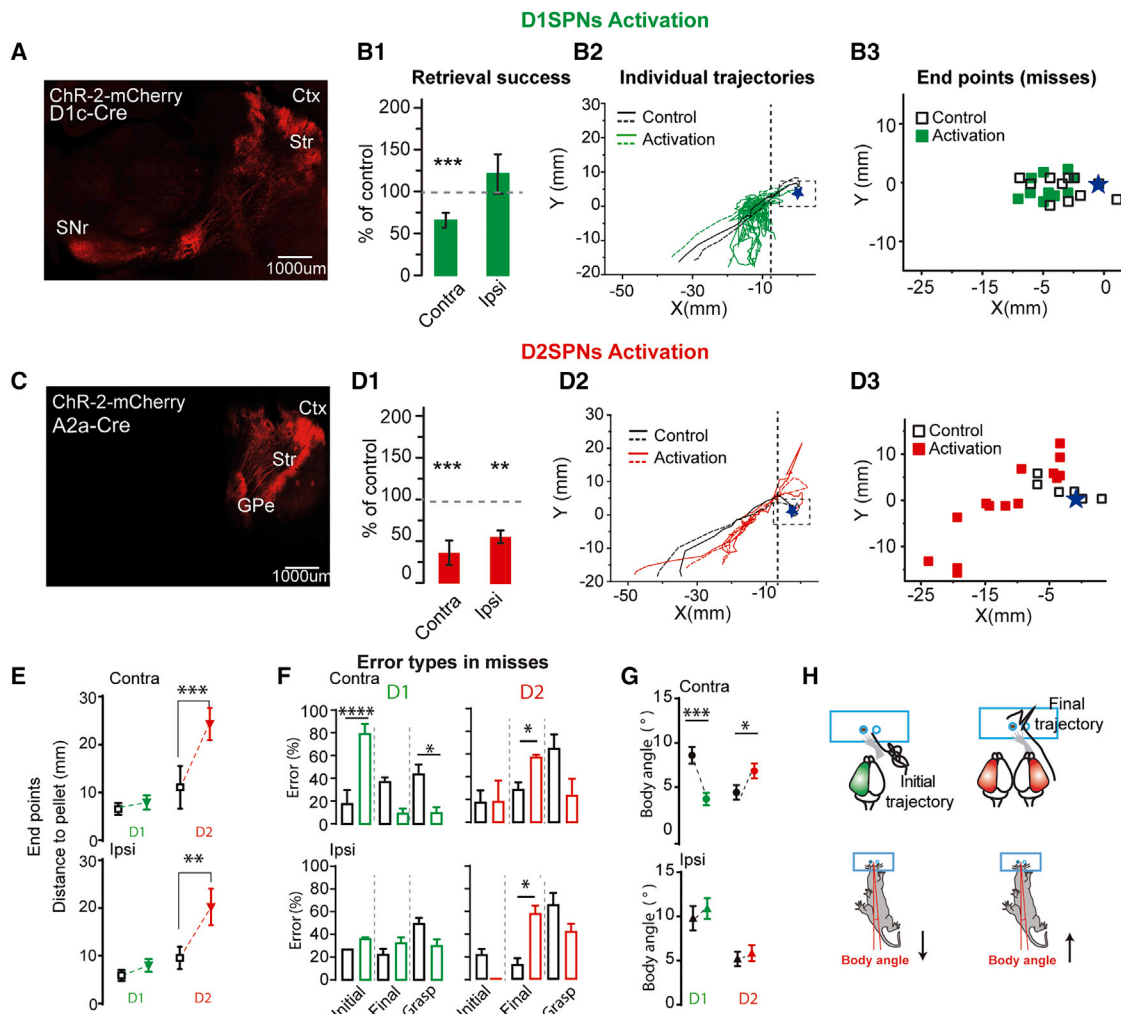
Figure 2. Optogenetic activation of D1 and D2 SPNs during reach-to-grasp actions

(A and C) Illustration of viral expression of ChR-2 carrying AAV viruses in sagittal sections from mice used in the experiments.

(B1 and D1) The success rate compared with control behavior for each mouse (Table 1; contra: D1 n = 5, D2 n = 4; ipsi: D1 n = 4, D2 n = 3 mice). Data plotted as mean ± SEM.

(B2 and D2) Paths of paws in hits and misses in two dimensions.

(B3, D3, and E) Plot of the end of each reach with respect to the target. The position of the pellet is denoted by a blue star. Distances by which animals missed the target are plotted in (E) for all 4 conditions: D1 contralateral control = 5.91 ± 18.6 mm, n = 18, stimulation = 7.06 ± 21.59 mm, n = 21 from 5 mice; D2 contralateral control = 9.38 ± 13.03, n = 21, stimulation = 23.36 ± 17.03, n = 28 from 4 mice (Mann-Whitney-Wilcoxon test U = 56.5, p = 0.0002); D1 ipsilateral control = 5.38 ± 15.8, n = 17, stimulation = 7.67 ± 26.2, n = 26 from 4 mice; D2 ipsilateral control = 6 ± 12.3, n = 19, stimulation = 23.36 ± 16.27, n = 18 from 3 mice (Mann-Whitney-Wilcoxon test U = 82, p = 0.0059). Data are presented as median ± interquartile range (IQR).

(F) Summary of the distributions of different kinds of errors for comparison with Figure 1E2. D1 contralateral type I error control = 18.2% ± 11.6%, stimulation = 79.9% ± 8.2% (Fisher's exact test, p < 0.0001); D2 contralateral type II error control = 23.6% ± 1.9%, stimulation = 58.8% ± 4.1% (Fisher's exact test, p = 0.0452). D2 ipsilateral type II error control = 12.8%, stimulation = 57.9% (Fisher's exact test, p = 0.0028; contra: D1 n = 5, D2 n = 4; ipsi: D1 n = 4, D2 n = 3 mice).

(G) Effects of optogenetic manipulation on body angle are plotted: D1 contralateral control = 8.58° ± 0.94°, n = 19, stimulation = 3.65° ± 0.7°, n = 19 from 5 mice (unpaired two-sample t test, t = 4.171, p = 0.0002); D2 contralateral control = 4.4° ± 0.52°, n = 19, stimulation = 6.8° ± 0.83°, n = 21 from 4 mice (unpaired two-sample t test, t = 2.415, p = 0.02); D1 ipsilateral control = 10.98° ± 1.3°, n = 20, stimulation = 11.83° ± 1.75°, n = 21 from 4 mice; D2 ipsilateral control = 5.65° ± 0.8°, n = 19, stimulation = 6.3° ± 0.9°, n = 22 from 3 mice. Data presented as mean ± SEM. Significant changes in posture are marked with an asterisk.

(H) Schematic summary of the different experimental manipulations.

See also Figure S2–S4.

compared with the control (Figure 2D1), but in this case, trajectories changed in the final phase of the reaching movement, with scattered endpoints away from the pellet in missed trials (Figure 2D2–2E, and S4). This led to a rise in final error type II (Figure 2G).

Comparison of results between contralateral activation of D1SPNs and D2SPNs highlight the functional relevance of both neuronal groups at different stages of the skilled movement (Figure 2H). However, our experimental design allowed us to examine ipsilateral influences on behavior.
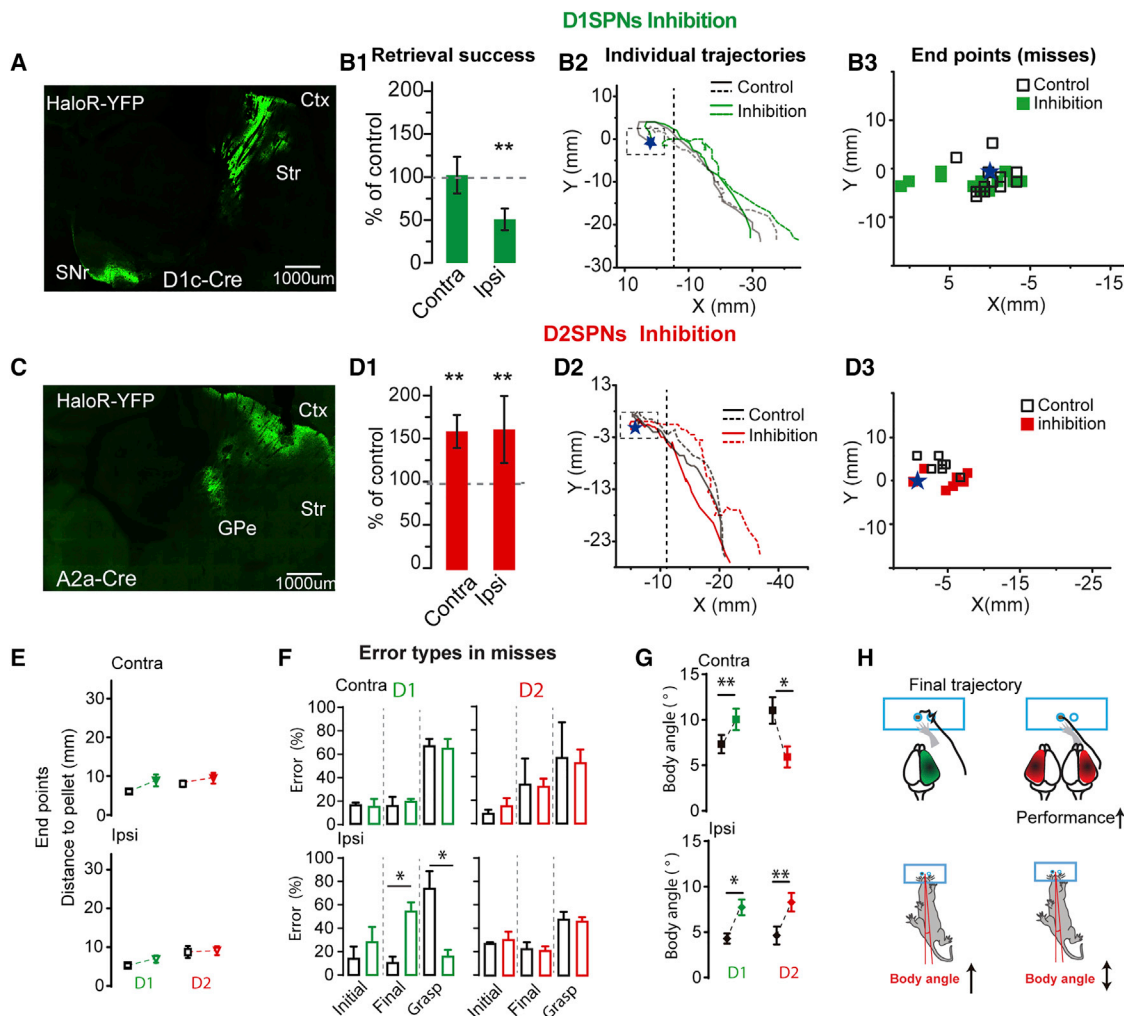
Figure 3. Optogenetic inhibition of D1 and D2 SPNs during reach-to-grasp actions

(A and C) Illustration of viral expression of HaloR carrying AAV viruses in sagittal sections from mice used in the experiments.

(B1 and D1) The average success rate compared with control behavior for each mouse (Table 1; contra: D1 n = 4, D2 n = 5; ipsi: D1 n = 5, D2 n = 3 mice). Data plotted as mean ± SEM.

(B2 and D2) Paths of paws in hits and misses in two dimensions.

(B3 and D3) The end of each reach with respect to the target. The position of the pellet is denoted by a blue star. Distances by which animals missed the target are plotted in (E) for all 4 conditions: D1 contralateral control = 6.08 ± 10.6 mm, n = 23, stimulation = 6.08 ± 25.93 mm, n = 27 from 4 mice; D2 contralateral control = 8.54 ± 22.18, n = 13, stimulation = 9.22 ± 23.61, n = 21 from 3 mice; D1 ipsilateral control = 4.73 ± 14.65, n = 26, stimulation = 5.55 ± 16.03, n = 24 from 5 mice; D2 ipsilateral control = 9.05 ± 10.92, n = 19, stimulation = 11.09 ± 23.1, n = 20 from 3 mice. Data are presented as median ± IQR.

(F) Distribution summary of kinds of errors for comparison with Figure 1E2. D1 ipsilateral error type II control = 10.9%, stimulation = 55% ± 7.1% (Fisher's exact test, p = 0.012) (contra: D1 n = 4, D2 n = 5; ipsi: D1 n = 5, D2 n = 3 mice).

(G) Effects of optogenetic manipulation on body angle are plotted: D1 contralateral control = 6.76° ± 1°, n = 20, stimulation = 10.49° ± 1.17°, n = 21 from 4 mice (unpaired two-sample t test, t = 2.73, p = 0.0099); D2 contralateral control = 10.79° ± 0.52°, n = 19, stimulation = 5.68° ± 1.16°, n = 15 from 5 mice (unpaired two-sample t test, t = 2.64, p = 0.012); D1 ipsilateral control = 4.05° ± 0.54°, n = 19, stimulation = 6.77° ± 0.85°, n = 19 from 5 mice (unpaired two sample t test, t = 2.67, p = 0.011); D2 ipsilateral control = 4.63° ± 0.74°, n = 20, stimulation = 9° ± 0.77°, n = 21 from 3 mice (unpaired two-sample t test, t = 4.061, p = 0.0002). Data are presented as mean ± SEM. Significant changes in body angle are marked with an asterisk.

(H) Schematic summary of the different experimental manipulations.

See also Figures S2–S4.

Ipsilateral D1SPN activation did not produce significant changes in retrieval success or the proportion of errors (Figure 2B1 and 2F). Nevertheless, when we compared the trajectories with PCA, we observed that trajectories in missed trials had a low percentage of overlap with the control cluster, indi-cating that ipsilateral D1SPN activation modified the reaching trajectory to some degree (Figures S2B and S3B). In contrast, ipsilateral D2SPN activation decreased retrieval success to 56.6% ± 7.6% of control values (Figure 2D1), and kinematic analyses showed changes similar to those during contralateral

activation (Figure 2E), consistent with final error type II (Figure 2G). These results show differential involvement of the two populations of SPNs in distinct phases of the skilled movement; although D1SPNs influence the initial reaching trajectory, D2SPNs have an effect in the final phase of the movement toward obtaining the goal. Moreover, importantly, our data on the two populations of SPN in hemispheres—ipsilateral and contralateral—relative to the preferred paw helped us disclose that unilateral forelimb movements require bilateral control.

Optogenetic inhibition

When we studied the effects of SPN inhibition in contralateral or ipsilateral hemispheres according to the preferred paw (Table 1), we observed that, in the contralateral hemisphere, D1SPN inhibition did not affect retrieval success or the proportion of error types (Figures 3B1 and 3G). However, comparison of trajectories in the PCA space showed little overlap of missed trials with the control cluster, indicating that, even though mice could perform the task, the trajectory they followed was different and more variable (Figure S2C). In contrast, contralateral and ipsilateral inhibition of D2SPNs induced an increase in retrieval success without changing the proportion of error types (Figures 3D1 and 3F; Table 1). In addition, PCA showed disparity between experimental and control trajectories (Figures S2D, S4C, and S4D). Basically, they exhibited variations in the initial phase of the movement with unaffected endpoints. Conceivably, contralateral inhibition of D2SPNs could have led to higher task efficiency by favoring the direct output pathway, whereas ipsilateral inhibition of D1SPNs could have produced a decrease in retrieval success attributable to an affected final trajectory and increased final error type II (Figures 3B1 and 3F), reminiscent of the effects of activation of D2SPNs (perhaps by disinhibition from D1SPNs). Our main findings, as summarized in Table 1, show opposite results for pellet retrieval success during activation compared with inhibition of D2SPNs on the ipsilateral or contralateral side to the preferred paw (Figures 2 and 3). In contrast, contralateral activation or ipsilateral inhibition of D1SPNs mainly resulted in unsuccessful pellet retrieval, likely making these neurons more involved in the reaching movement itself. Usually, data resulting from photomodulation could be explained partially by specific combinations of movement errors, although some results can be best appreciated as arising from several factors combined, as indicated by PCA (Table 1; Figures 2 and 3).

Measurements of body posture

Considering that the animals' posture was different in successful and failed reaches under control conditions (Figure 1) and that a simple explanation for involvement of the ipsilateral hemisphere in reaching could be posture, we measured body angle during optogenetic activation on the hemisphere ipsilateral or contralateral to the preferred paw. However, we observed that contralateral manipulations affected posture the most. Contralateral photoactivation of D1 neurons revealed significant changes in body angle: a decrease during activation and an increase during inhibition (Figures 2G, 2H, 3G, and 3H). With contralateral activation of D2 neurons, only a small increase in

body posture was observed, whereas ipsilateral inhibition generated opposite effects dependent on the inhibited hemisphere; namely, a decrease during contralateral and an increase during ipsilateral photoinhibition (Figures 2 and 3).

These diverse changes in posture show that the effects of ipsilateral optogenetic manipulations on reaching could not be explained simply by the changes in body angle we measured.

Ex vivo recordings of untrained control mice and SPN connectivity in the dorsolateral striatum

We performed patch-clamp recordings from SPNs in D1-Cre and A2a-Cre mice in which fluorescent ChR-2 was expressed. Fluorescent and non-fluorescent D1 and D2 neurons displayed typical SPN electrophysiological characteristics, and post hoc staining of biocytin-filled cells confirmed their morphological signatures and identities (Figures 4A and 4B). Connectivity patterns between SPNs were studied in voltage-clamp recordings of inhibitory postsynaptic currents (IPSCs) evoked by optical stimulation while holding neurons at +20 mV (ChR-2 photocurrent reversal potential) (Method details: Stimulation).

D1SPN-D1SPN connections tested in D1-Cre mice showed IPSCs with a median amplitude of 70 pA (n = 8/8; 100% of neurons produced detectable responses; Figures 4C, 4H, and 4D). To our surprise, when we tested D1SPN-D2SPN connectivity, reported previously to be low or non-existent (Koos et al., 2004; Taverna et al., 2004; Tunstall et al., 2002), we were able to evoke IPSCs in D2SPN mCherry (−) cells with an amplitude of 56 pA, although fewer cells had detectable responses (n = 8/20, 40%; Figures 4E and 4H). IPSCs remained unchanged after application of the glutamate receptor blockers NBQX (10 μM) and APV (50 μM), confirming that responses were not due to cortical expression of ChR-2 driven by D1-Cre (n = 7 neurons; Figure S5A). It may be that low connectivity rates explain the difficulty in finding connections with typical paired recordings. D2SPN-D2SPN functional connectivity studied in A2a-Cre mice evoked IPSCs in 11 of 12 recorded cells with a median amplitude of 46 pA. When we recorded putative D2SPN-D1SPN mCherry (−) cells, we were able to evoke robust IPSCs in 88% of cells (58 pA amplitude; n = 16/18; Figures 4F and 4G). IPSC amplitude among all cell populations was similar (Figure 4H). IPSC kinetics differed depending on the target neuron. Rise and decay times were significantly slower when the recorded neuron belonged to the same population; i.e., D1-D1 and D2-D2. In these cases, recorded cells also expressed ChR-2, and although we compensated for voltage activation with light, channels that remained opened may have distorted the timescale of the responses (Figures 4D, 4G, S5C, and S5D; Methods details: Stimulation).

The effect of SPN collateral inhibition on action potential firing was studied with depolarizing current steps to threshold (−45 mV). Strikingly, as addressed in the Discussion (Interplay between D1SPNs and D2SPNs), the signals IPSCs evoked by single photostimulus (5 ms, 0.5 Hz, 900 μW) delivered to neighboring D1SPNs were strong enough to delay or even suppress firing (Figures 4I and 4J), an outcome that has been proven previously to be elusive with techniques involving paired recordings (Koos et al., 2004; Tepper et al., 2008).
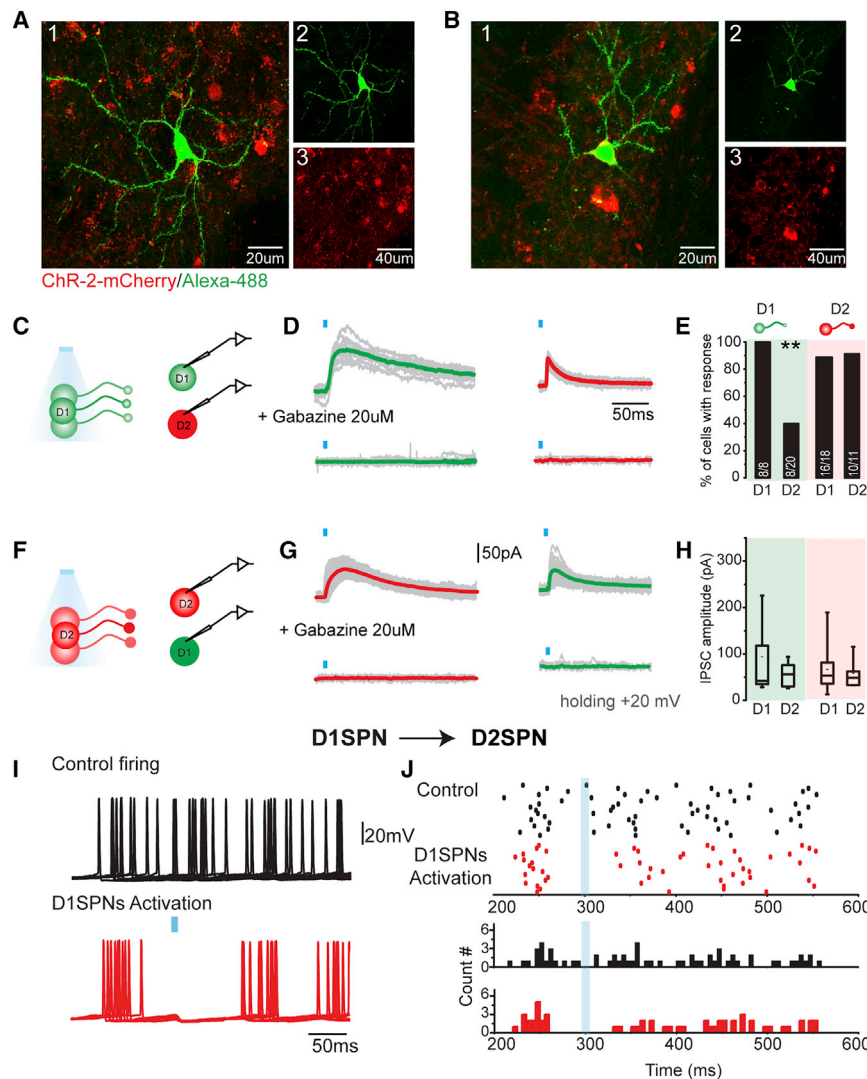
Figure 4. *Ex vivo* recordings of untrained control mice and SPN connectivity in the dorsolateral striatum

(A and B) Cells targeted for electrophysiological recordings from D1SPNs and D2SPNs Shown are examples of SPNs filled with biocytin (green) during recording of ChR2-mCherry (−) (A) and ChR-2-mCherry (+) (B).

(C) Schematic representation of the recording/stimulation protocol.

(D) Inhibitory postsynaptic currents (IPSCs) recorded in D1SPNs (green) and D2SPNs (red), evoked by photostimulation of D1SPNs (D1SPN-to-D1SPN and D1SPN-to-D2SPN connections). Data plotted as mean ± SEM.

(E) Summary of the percentage of connectivity of D1SPN and D2SPN IPSCs and summary of IPSC amplitude (Kruskal-Wallis ANOVA, χ^2 [df 3] = 0.93, p = 0.86).

(F) Schematic representation of the recording/stimulation protocol.

(G) IPSCs evoked by photostimulation of D2SPNs recorded in a D2SPN (red) and in a D1SPN (green). Bottom: blockade of IPSCs in the presence of the GABA$_A$ receptor antagonist gabazine (20 μM). The blue bar indicates the time of stimulation.

(H) Summary of IPSC amplitude for all experiments. D1-Cre, n = 11; A2a-Cre, n = 12 mice.

(I) Collateral connectivity exerts strong inhibition on action potential firing of neighboring SPNs. Action potentials were evoked by a depolarizing current pulse. Shown are 10 overlapping traces for control firing and D1SPN activation.

(J) Photoactivation of neighboring D1SPNs expressing ChR2-mCherry completely abolished evoked spikes in the recorded D2SPNs.

See also Figure S5.

7; Figures 5G and 5H; Table S1). Median IPSC amplitude increased significantly only in the ipsilateral hemisphere (174 pA) compared with contralateral (73 pA) and control conditions (70.5 pA) (Figure 5H). After learning, IPSC kinetics did not differ significantly in any recorded D1SPNs (Figures S5C and S5D).

In contrast, after learning, ipsilateral connectivity detected between D2SPNs-D1SPNs decreased significantly to 46.6% (n = 7/15), whereas the percentage of cells with detectable responses on the contralateral side (79%, n = 15/19) remained similar to control conditions (88%) (Figures 6A–6C). IPSC amplitude increased in both hemispheres to 109 pA contralaterally and 115 pA ipsilaterally compared with 58 pA under control conditions (Figure 6D; Table S1), but IPSC kinetics did not vary (Figures S5C and S5D). Connectivity and IPSC amplitude between ipsilateral and contralateral D2SPNs-D2SPNs were not modified significantly (Figures 6E–6H).

In summary, our findings regarding functional connectivity highlight a dynamic interplay between SPNs of different classes (D1 and D2) (Figures 5D and 6D) that changes after learning and performing a skilled forelimb task. The major changes show an increase in inhibitory control by D1 neurons over D2 ipsilaterally and D2 to D1 contralaterally. The small D1-D2 effects in controls

Functional connectivity of D1SPNs after learning a skilled motor behavior

Corticostriatal plasticity after learning has been measured recently *ex vivo* by inducing local evoked field potentials (LTP and LTD) (Hawes et al., 2015; Yin et al., 2009b). Here we recorded IPSCs evoked with widespread optogenetic stimulation of D1SPNs in putative mCherry (−) D2SPNs or mCherry (+) D1SPNs from 15 trained D1-Cre mice. Approximately 1 h after the last session of behavioral testing, brain slices were made, and experiments were performed as above.

D1SPN-to-D2SPN responses increased on the ipsilateral side, with 73.3% of cells receiving connections (n = 11/15) compared with 39% of cells (n = 7/18) on the contralateral side (40% in controls) (Figures 5A–5C; Table S1). Compared with a control median amplitude of 56 pA, ipsilateral IPSC amplitude increased to 63 pA and decreased significantly on the contralateral side to 28 pA (Figure 5D). We found no differences in connectivity rate among D1SPN-D1SPN connections between 87.5% (n = 7/8) ipsilateral and 100% contralateral sides (n = 7/
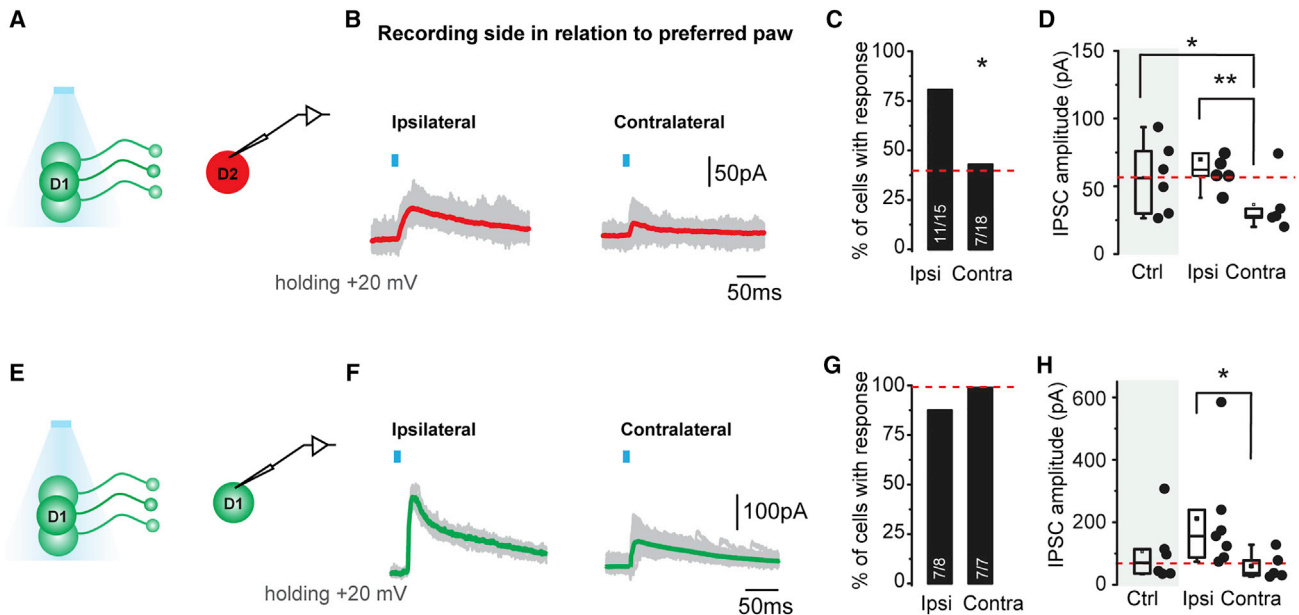
Figure 5. Functional connectivity of D1SPNs after learning a skilled motor behavior

(A) Schematic representation of the recording/stimulation protocol.

(B) IPSCs evoked by photostimulation of D1SPNs recorded in D2SPNs from ipsilateral and contralateral sides in relation to the preferred paw after learning a skilled motor behavior.

(C and D) Summary of IPSC recordings, percentage of connectivity (χ^2 [df 1] = 4.97, p = 0.025) (C), and box plots of IPSC amplitude (D) from ipsilateral and contralateral sides after learning the single-pellet grasping task (Mann-Whitney-Wilcoxon test control versus ipsi U = 19, p = 0.5728; control versus contra, U = 6, p = 0.033; ipsi versus contra, U = 6, p = 0.0093).

(E) Schematic representation of the recording/stimulation protocol.

(F) IPSCs evoked by photostimulation of D1SPNs recorded in D1SPNs from ipsilateral and contralateral sides in relation to the preferred paw after learning a skilled motor behavior.

(G and H) Summary of the percentages of connectivity and (H) box plots of IPSC amplitude from control mice and ipsilateral and contralateral sides after learning the single-pellet grasping task (Mann-Whitney-Wilcoxon test, control versus ipsi, U = 8, p = 0.47; control versus contra, U = 19, p = 0.83; ipsi versus contra, U = 31, p = 0.045). Data are from 15 D1-Cre trained mice. The blue bar indicates the time of stimulation. The dotted line represents the median of control conditions. See also Figure S5 and Table S1.

become even smaller contralaterally, whereas D2 to D1 becomes half as common but twice as strong ipsilaterally.

DISCUSSION

Our results suggest different roles for the two pathways during reaching to grasp chocolate-flavored food pellets. They highlight the contributions of both hemispheres in skilled performance and demonstrate that learned skills are associated with synaptic changes. They also emphasize, as shown by others, that balanced activity and interplay between D1SPNs and D2SPNs is essential for striatal influence on motor programs (Barbera et al., 2016; Gerfen et al., 1990; Kravitz et al., 2010; Tecuapetla et al., 2016; Yttri and Dudman, 2016).

We imagine that intentional movement is modulated by striatal activity that involves ensembles of neurons comprising D1SPNs and D2SPNs. Nevertheless, we tried to distinguish the roles of each subgroup of neurons by inhibiting or exciting them individually during performance of a skilled movement. Although we used continuous stimulation for these studies, our own previous work using slices showed that at least half of the cells tested were still firing after 30 s of continuous stimulation (Jáidar

et al., 2019). The timescale of excitation or inhibition might not extend to the whole stimulation period or to every cell in the striatal region, but we interpret our results, as have others (Kravitz et al., 2010), as a net increase after channel rhodopsin and a net decrease after halorhodopsin activation.

Interplay between D1SPNs and D2SPNs

Balanced activity between SPNs starts in the striatal microcircuitry, where they interconnect via axon collaterals to exert lateral inhibition (López-Huerta et al., 2013; Taverna et al., 2008; Tepper et al., 2008). Collateral inhibition has long been hypothesized to be the main source of firing control because of neuronal branching within the striatum; however, until recently, there has been little evidence demonstrating that collateral inhibition suppresses action potential firing in neighboring neurons (Tecuapetla et al., 2016; Tepper et al., 2008; Wilson, 2007). Here we describe inhibition of individual neurons after optical activation of others in the neighborhood, suggesting that the previous difficulty in measuring the effects of the collaterals resulted from restricting stimulation to single neurons when direct connections are rare (Jaeger et al., 1994; Tunstall et al., 2002). Work by Lemos et al. (2016) shows that other
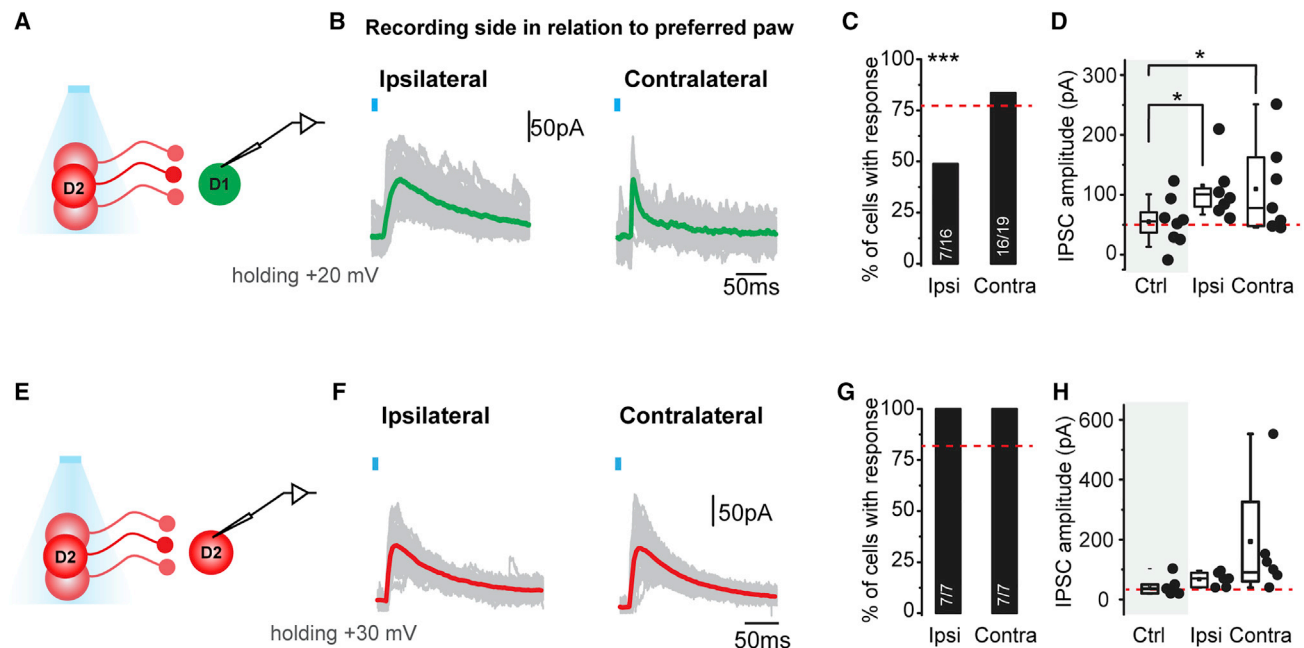
Figure 6. Functional connectivity of D2SPNs after learning a skilled motor behavior

(A) Schematic representation of the recording/stimulation protocol.

(B) IPSCs evoked by photostimulation of D1SPNs recorded in D2SPNs from ipsilateral and contralateral sides in relation to the preferred paw after learning a skilled motor behavior.

(C and D) Summary of IPSC recordings, percentage of connectivity (χ^2 [df 1] = 7.767, p = 0.005) (C), and box plots of IPSC amplitude (D) from ipsilateral and contralateral sides after learning the single-pellet grasping task (Mann-Whitney-Wilcoxon test control versus ipsi, U = 24.5, p = 0.034; control versus contra, U = 52, p = 0.04; ipsi versus contra, U = 41, p = 0.94).

(E) Schematic representation of the recording/stimulation protocol.

(F) IPSCs evoked by photostimulation of D2SPNs recorded in D2SPNs from ipsilateral and contralateral sides in relation to the preferred paw after learning a skilled motor behavior.

(G and H) Summary of IPSC recordings, percentage of connectivity (G), and box plots of IPSC amplitude (H) from ipsilateral and contralateral sides after learning the single-pellet grasping task (Mann-Whitney-Wilcoxon test control versus ipsi, U = 14, p = 0.21; control versus contra, U = 12, p = 0.13; ipsi versus contra, U = 15, p = 0.66). Data are from 14 A2a-Cre trained mice. The blue bar indicates the time of stimulation. The dotted line represents the median of control conditions. See also Figure S5 and Table S1.

sources of GABA may also be activated when D2SPNs are reduced in activity *in vivo*, suggesting that there are more ways for the two groups SPNs to interact than the direct connections we measured. Indeed, it is clear that interactions outside of the striatum are involved in the effects we see in behaving animals.

Under control conditions, our results agree with earlier work (Taverna et al., 2004) showing that D1SPNs display low connectivity with D2SPNs. Moreover, after training, ipsilateral and contralateral hemispheres display activity-dependent plasticity related to the learned motor task. This plasticity is perhaps derived similarly to that described previously for excitatory synapses (Kozorovitskiy et al., 2012; Picazo et al., 2009; Xu et al., 2009). After training, D1SPNs increase connectivity and strength ipsilaterally, which is probably linked to unexplored participation of the ipsilateral striatum in skilled movement driven by cortical activity (Verstynen et al., 2005). D2SPNs decrease connectivity on the ipsilateral side but increase the current in the remaining connections, an obvious way to select neurons to be part of appropriate ensembles for fine control. Contralaterally, D2SPNs have more powerful inhibitory actions, whereas D1SPNs are less effective.

The role of contralateral striatal subpopulations

It is likely that selection of motor programs for smooth movement performance is tightly regulated so that only a few specialized "action" ensembles become active (Cui et al., 2013). Our behavioral experiments indicate that contralateral activation of D1SPNs disturbs movement kinematics (Figure 2B2); an animal makes multiple attempts to reach, suggesting that interference by light-activated "extra" motor programs results in multiple interruptions in movement.

Surprisingly, when we inhibit contralateral D1SPNs, we see a similar effect on kinematics, as if inhibition and excitation produce similar results. Perhaps excitation and inhibition disrupt the effective ensembles of striatal neurons so that effects of optogenetic actions are on the ensemble dynamics and not exclusively on the actions of one kind of output. However, we do see a significant effect of ipsilateral D1SPN inhibition on reaching accuracy, presumably because disinhibition of D2SPNs has spread local targeting of reaching movement (final error type II). Indeed, our optogenetic stimulation of contralateral D2SPNs leads to errors in trajectory right before grasping (missed target position type II error), reinforcing the idea that their role is in targeting of the reach. Optogenetic inhibition of D2SPNs leads to

better performance without major changes in trajectory. Inhibition of a strong indirect pathway is likely to enhance the signal-to-noise ratio of existing ensembles, resulting in more consistent performance from trial to trial (Dudman and Krakauer, 2016). Indeed, it is striking that inhibition of D2SPNs on both sides of the brain improves performance (Figure 3D1).

Although forelimb trajectories observed during striatal optogenetic stimulation or inhibition are dispersed to different degrees, manipulation of contralateral D1SPNs induced dramatic disturbances in movement. This effect resembles alterations resulting from increased D1-mediated neurotransmission thought to be responsible for L-dopa-induced dyskinesias (Aubert et al., 2005; Farré et al., 2015). The dopamine system is intact in our animals, and the only "dyskinesia" we observed was linked to movement of the trained paw during optogenetic action. Our data suggest that, for the reach-to-grasp task, contralateral D1SPNs direct the movement during reaching, whereas D2SPNs filter overall striatal activity so that essential motor programs are activated to achieve the grasp.

The role of ipsilateral striatal subpopulations

Slice experiments demonstrate that D1SPN-D2SPN connectivity is increased on the ipsilateral side, leading to upregulation of direct pathway output. This upregulation may explain why further activation of D1SPNs on the ipsilateral side during behavioral experiments does not affect reaching success. Perhaps overactivation by optogenetic manipulation cannot affect the already established intrastriatal ensemble selection (Barbera et al., 2016); however, optogenetic inhibition of D1SPNs probably suppresses motor programs that help with smooth delivery of the task (Dudman and Krakauer, 2016). In the case of the indirect pathway, we observe alterations similar to those on the contralateral side.

As with the improved success rate of pellet retrieval (>60%) resulting from dorsolateral D2SPN inhibition, skilled forepaw use can be improved with striatal neurotoxic lesions (Whishaw et al., 2007) or unilateral intrastriatal depletion of dopamine (Evenden and Robbins, 1984). Enhanced performance could result from increased sensorimotor cortical input to the dorsolateral striatum (Graybiel, 2008; Yin et al., 2009b) or perhaps to D2SPN-induced functional decoupling of competing motor behaviors (Cui et al., 2013; Mink, 1996). Our *in vivo* optogenetic manipulation experiments with *ex vivo* electrophysiological data highlight the importance of intrastriatal microcircuit computations for final motor output. Although we observe that both hemispheres participate in motor control of the limb in motion, the contralateral side always had a greater influence on the performance. Successful performance of skilled movement requires a fine balance between the two pathways and correct selection of ensembles in contralateral and ipsilateral hemispheres. These data show specific roles not only for both types of SPNs but for each hemisphere during skilled motor performance.

With these results, we hypothesize that ipsilateral D1SPNs are needed to control fine motor programs required throughout skilled motor performance, whereas D2SPNs balance the activity among striatal ensembles in control of target accuracy.

Effects on body posture

Even though mice used only their preferred paws to execute the task, reaching requires whole-body coordination. In fact, contralateral activation of both output pathways led to changes in body angle during missed trials, perhaps to compensate for movement deficits. Ipsilateral manipulations of D1SPNs affected interlimb coordination, manifested by changes in stance length. D2SPN inhibition of both hemispheres induced opposite changes in body angle. This suggests that both hemispheres control aspects of body posture as well as paw movement during action.

In conclusion, dorsolateral striata of both hemispheres participate in control of unilateral forelimb movement. D1SPN output is upregulated by training in the ipsilateral hemisphere and downregulated in the contralateral hemisphere. In contrast, D2SPN output is downregulated on the ipsilateral side and upregulated on the contralateral side.

Interpretive model

Our results highlight the need for important missing experimental evidence and prompt us to propose a hypothesis and an interpretive model for further research.

Hypothesis

Changes in collateral inhibitory strength reflect formation of different cell assemblies that sculpt motor program parameters for reaching movement. Based on reports that both sides of the brain are involved in unilateral movements (Davare et al., 2007; Ganguly et al., 2009; van den Berg et al., 2011), we generated an entirely new set of control data with which to compare our trained experimental animals to estimate connectional differences between control and experimental animals. This helped us demonstrate that connectivity between striatal cells in trained animals changes significantly in both hemispheres. Confirmation of the importance of these changes in connectivity on behavior would require *in vivo* study of the connectivity of individual cells directly involved in executing the action.

The fact that the changes in circuitry along with the changes from optogenetic manipulations are present bilaterally indicates that control of reaching involves both striata not only in postural adjustment but in the movement itself.

Model

Recent evidence implies that the two types of SPNs act together in executing movement (Markowitz et al., 2018; Sheng et al., 2019) and separately in different temporal sequences (Ardid et al., 2019). Accordingly, our results indicate that D1SPNs are clearly involved in the early parts of the reaching movement (trajectory) and that excitation of D2SPNs results in disrupted targeting in the later parts of the reach.

Our model proposes that the whole skilled movement is executed by assemblies of SPNs generated by their glutamatergic inputs containing differences in connectivity patterns between the two groups (Assous et al., 2019; Assous and Tepper, 2019; Lee et al., 2017). These assemblies presumably code for changes in both sides of the brain and musculature involved in movements specific for the task. Within the assemblies, it seems likely that D1SPNs are mainly involved in initiation of reach and control of its initial trajectory. When the movement sequence is started, D2SPNs are involved mainly in accuracy of attaining

the goal (avoiding error type II). The changes in connectivity between SPNs we observed in electrophysiology provide a clue regarding the relationships developed between SPN assemblies in performance of the task. We propose, in this model, that the observed reduction of D1SPN-D1SPN inhibition (Figure 5D) allows participation of a larger group of D1SPNs in the assembly. Moreover, as the movement approaches its target, we speculate that the observed increase in D2SPN-to-D1SPN inhibition (Figure 6D) may possibly lead to refinement of the ensemble until increased D2SPN-to-D2SPN inhibition (Figure 6 H) provides the final approach. Although the detailed actions of the ipsilateral striatum are still a mystery, it might be possible that, along with the training, modifications in the collateral effectiveness take place.

Recent experiments suggest a much more dynamic influence of higher centers in the brain over even simple movements, indicating that even reflex movements can be modified in humans by cognitive processes involving the consequences of the movement (Carroll et al., 2019). Perhaps controlling such processes is a function of D2SPNs so that silencing them during movement increases retrieval success by removing distractions, providing animals are well trained. Conversely, exciting this pathway induces error in the movement, resulting in disruption of the final trajectory (Table 1). Clearly, future experiments *in vivo* and computational verification of interplay between the two pathways are required to adequately test these ideas.

STAR★METHODS

Detailed methods are provided in the online version of this paper and include the following:

- KEY RESOURCE TABLE
- RESOURCE AVAILABILITY
  - Lead contact
  - Materials availability
  - Data and code availability
- EXPERIMENTAL MODEL AND SUBJECT DETAILS
- METHOD DETAILS
  - AAV expression and stereotaxic surgery
  - Single-pellet, reach-to-grasp task
  - Kinematic quantification of reaching
  - Slice preparation
  - Electrophysiological recordings
  - Stimulation
  - Drugs
  - Histology
- QUANTIFICATION AND STATISTICAL ANALYSIS

SUPPLEMENTAL INFORMATION

Supplemental Information can be found online at https://doi.org/10.1016/j.celrep.2020.108651.

AUTHOR CONTRIBUTIONS

Conceptualization, V.G.L.-H. and G.W.A.; Methodology, V.G.L.-H., J.A.D., and G.W.A.; Formal Analysis, V.G.L.-H. and J.A.D.; Investigation, V.G.L.-H.; Resources, Y.N. and O.J.; Writing – Original Draft, V.G.L.-H.; Writing – Reviewing & Editing, V.G.L.-H., J.A.D., M.G.M., and G.W.A.

DECLARATION OF INTERESTS

The authors declare no competing interests.

REFERENCES

Ardid, S., Sherfey, J.S., McCarthy, M.M., Hass, J., Pittman-Polletta, B.R., and Kopell, N. (2019). Biased competition in the absence of input bias revealed through corticostriatal computation. Proc. Natl. Acad. Sci. USA 116, 8564–8569.

Assous, M., and Tepper, J.M. (2019). Excitatory extrinsic afferents to striatal interneurons and interactions with striatal microcircuitry. Eur. J. Neurosci. 49, 593–603.

Assous, M., Dautan, D., Tepper, J.M., and Mena-Segovia, J. (2019). Pedunculopontine glutamatergic neurons provide a novel source of feedforward inhibition in the striatum by selectively targeting interneurons. J. Neurosci. 39, 4727–4737.

Aubert, I., Guigoni, C., Håkansson, K., Li, Q., Dovero, S., Barthe, N., Bioulac, B.H., Gross, C.E., Fisone, G., Bloch, B., and Bezard, E. (2005). Increased D1 dopamine receptor signaling in levodopa-induced dyskinesia. Ann. Neurol. 57, 17–26.

Azim, E., Fink, A.J., and Jessell, T.M. (2014). Internal and External Feedback Circuits for Skilled Forelimb Movement. Cold Spring Harb. Symp. Quant. Biol. 79, 81–92.

Barbera, G., Liang, B., Zhang, L., Gerfen, C.R., Culurciello, E., Chen, R., Li, Y., and Lin, D.T. (2016). Spatially Compact Neural Clusters in the Dorsal Striatum Encode Locomotion Relevant Information. Neuron 92, 202–213.

Brus-Ramer, M., Carmel, J.B., and Martin, J.H. (2009). Motor cortex bilateral motor representation depends on subcortical and interhemispheric interactions. J. Neurosci. 29, 6196–6206.

Carroll, T.J., McNamee, D., Ingram, J.N., and Wolpert, D.M. (2019). Rapid Visuomotor Responses Reflect Value-Based Decisions. J. Neurosci. 39, 3906–3920.

Cui, G., Jun, S.B., Jin, X., Pham, M.D., Vogel, S.S., Lovinger, D.M., and Costa, R.M. (2013). Concurrent activation of striatal direct and indirect pathways during action initiation. Nature 494, 238–242.

d'Avella, A., Saltiel, P., and Bizzi, E. (2003). Combinations of muscle synergies in the construction of a natural motor behavior. Nat. Neurosci. 6, 300–308.

Davare, M., Duque, J., Vandermeeren, Y., Thonnard, J.L., and Olivier, E. (2007). Role of the ipsilateral primary motor cortex in controlling the timing of hand muscle recruitment. Cereb. Cortex 17, 353–362.

Donchin, O., Gribova, A., Steinberg, O., Bergman, H., and Vaadia, E. (1998). Primary motor cortex is involved in bimanual coordination. Nature 395, 274–278.

Dudman, J.T., and Krakauer, J.W. (2016). The basal ganglia: from motor commands to the control of vigor. Curr. Opin. Neurobiol. 37, 158–166.

Evenden, J.L., and Robbins, T.W. (1984). Effects of unilateral 6-hydroxydopamine lesions of the caudate-putamen on skilled forepaw use in the rat. Behav. Brain Res. *14*, 61–68.

Farré, D., Muñoz, A., Moreno, E., Reyes-Resina, I., Canet-Pons, J., Dopeso-Reyes, I.G., Rico, A.J., Lluís, C., Mallol, J., Navarro, G., et al. (2015). Stronger Dopamine D1 Receptor-Mediated Neurotransmission in Dyskinesia. Mol. Neurobiol. *52*, 1408–1420.

Franklin, K.B.J., and Paxinos, G. (2008). The Mouse Brain in Stereotaxic Coordinates, Third Edition (Elsevier).

Ganguly, K., Secundo, L., Ranade, G., Orsborn, A., Chang, E.F., Dimitrov, D.F., Wallis, J.D., Barbaro, N.M., Knight, R.T., and Carmena, J.M. (2009). Cortical representation of ipsilateral arm movements in monkey and man. J. Neurosci. *29*, 12948–12956.

Gerfen, C.R., Engber, T.M., Mahan, L.C., Susel, Z., Chase, T.N., Monsma, F.J., Jr., and Sibley, D.R. (1990). D1 and D2 dopamine receptor-regulated gene expression of striatonigral and striatopallidal neurons. Science *250*, 1429–1432.

Gradinaru, V., Zhang, F., Ramakrishnan, C., Mattis, J., Prakash, R., Diester, I., Goshen, I, Thompson, K.R., and Deisseroth, K. (2010). Molecular and cellular approaches for diversifying and extending optogenetics. Cell *141*, 154–165.

Graybiel, A.M. (2008). Habits, rituals, and the evaluative brain. Annu. Rev. Neurosci. *31*, 359–387.

Hawes, S.L., Evans, R.C., Unruh, B.A., Benkert, E.E., Gillani, F., Dumas, T.C., and Blackwell, K.T. (2015). Multimodal Plasticity in Dorsal Striatum While Learning a Lateralized Navigation Task. J. Neurosci. *35*, 10535–10549.

Jaeger, D., Kita, H., and Wilson, C.J. (1994). Surround inhibition among projection neurons is weak or nonexistent in the rat neostriatum. J. Neurophysiol. *72*, 2555–2558.

Jáidar, O., Carrillo-Reid, L., Nakano, Y., Lopez-Huerta, V.G., Hernandez-Cruz, A., Bargas, J., Garcia-Munoz, M., and Arbuthnott, G.W. (2019). Synchronized activation of striatal direct and indirect pathways underlies the behavior in unilateral dopamine-depleted mice. Eur. J. Neurosci. *49*, 1512–1528.

Koos, T., Tepper, J.M., and Wilson, C.J. (2004). Comparison of IPSCs evoked by spiny and fast-spiking neurons in the neostriatum. J. Neurosci. *24*, 7916–7922.

Kozorovitskiy, Y., Saunders, A., Johnson, C.A., Lowell, B.B., and Sabatini, B.L. (2012). Recurrent network activity drives striatal synaptogenesis. Nature *485*, 646–650.

Kravitz, A.V., Freeze, B.S., Parker, P.R., Kay, K., Thwin, M.T., Deisseroth, K., and Kreitzer, A.C. (2010). Regulation of parkinsonian motor behaviours by optogenetic control of basal ganglia circuitry. Nature *466*, 622–626.

Lee, C.T., Bendriem, R.M., Wu, W.W., and Shen, R.F. (2017). 3D brain Organoids derived from pluripotent stem cells: promising experimental models for brain development and neurodegenerative disorders. J. Biomed. Sci. *24*, 59.

Lemos, J.C., Friend, D.M., Kaplan, A.R., Shin, J.H., Rubinstein, M., Kravitz, A.V., and Alvarez, V.A. (2016). Enhanced GABA Transmission Drives Bradykinesia Following Loss of Dopamine D2 Receptor Signaling. Neuron *90*, 824–838.

Li, N., Daie, K., Svoboda, K., and Druckmann, S. (2016). Robust neuronal dynamics in premotor cortex during motor planning. Nature *532*, 459–464.

López-Huerta, V.G., Carrillo-Reid, L., Galarraga, E., Tapia, D., Fiordelisio, T., Drucker-Colin, R., and Bargas, J. (2013). The balance of striatal feedback transmission is disrupted in a model of parkinsonism. J. Neurosci. *33*, 4964–4975.

Lopez-Huerta, V.G., Nakano, Y., Bausenwein, J., Jaidar, O., Lazarus, M., Cherassse, Y., Garcia-Munoz, M., and Arbuthnott, G. (2016). The neostriatum: two entities, one structure? Brain Struct. Funct. *221*, 1737–1749.

MacLellan, C.L., Gyawali, S., and Colbourne, F. (2006). Skilled reaching impairments follow intrastriatal hemorrhagic stroke in rats. Behav. Brain Res. *175*, 82–89.

Markowitz, J.E., Gillis, W.F., Beron, C.C., Neufeld, S.Q., Robertson, K., Bhagat, N.D., Peterson, R.E., Peterson, E., Hyun, M., Linderman, S.W., et al. (2018). The Striatum Organizes 3D Behavior via Moment-to-Moment Action Selection. Cell *174*, 44–58.e17.

Marques, J.M., and Olsson, I.A. (2010). Performance of juvenile mice in a reach-to-grasp task. J. Neurosci. Methods *193*, 82–85.

Miklyaeva, E.I., Castañeda, E., and Whishaw, I.Q. (1994). Skilled reaching deficits in unilateral dopamine-depleted rats: impairments in movement and posture and compensatory adjustments. J. Neurosci. *14*, 7148–7158.

Mink, J.W. (1996). The basal ganglia: focused selection and inhibition of competing motor programs. Prog. Neurobiol. *50*, 381–425.

Morris, B.T., and Trivedi, M.M. (2011). Trajectory learning for activity understanding: unsupervised, multilevel, and long-term adaptive approach. IEEE Trans. Pattern Anal. Mach. Intell. *33*, 2287–2301.

Overduin, S.A., d'Avella, A., Carmena, J.M., and Bizzi, E. (2012). Microstimulation activates a handful of muscle synergies. Neuron *76*, 1071–1077.

Picazo, O., Chuc-Meza, E., Anaya-Martinez, V., Jimenez, I., Aceves, J., and Garcia-Ramirez, M. (2009). 6-Hydroxydopamine lesion in thalamic reticular nucleus reduces anxiety behaviour in the rat. Behav. Brain Res. *197*, 317–322.

Schneider, F., Grimm, C., and Hegemann, P. (2015). Biophysics of Channelrhodopsin. Annu. Rev. Biophys. *44*, 167–186.

Sheng, M.J., Lu, D., Shen, Z.M., and Poo, M.M. (2019). Emergence of stable striatal D1R and D2R neuronal ensembles with distinct firing sequence during motor learning. Proc. Natl. Acad. Sci. USA *116*, 11038–11047.

Taverna, S., van Dongen, Y.C., Groenewegen, H.J., and Pennartz, C.M. (2004). Direct physiological evidence for synaptic connectivity between medium-sized spiny neurons in rat nucleus accumbens in situ. J. Neurophysiol. *91*, 1111–1121.

Taverna, S., Ilijic, E., and Surmeier, D.J. (2008). Recurrent collateral connections of striatal medium spiny neurons are disrupted in models of Parkinson's disease. J. Neurosci. *28*, 5504–5512.

Tecuapetla, F., Matias, S., Dugue, G.P., Mainen, Z.F., and Costa, R.M. (2014). Balanced activity in basal ganglia projection pathways is critical for contraversive movements. Nat. Commun. *5*, 4315.

Tecuapetla, F., Jin, X., Lima, S.Q., and Costa, R.M. (2016). Complementary Contributions of Striatal Projection Pathways to Action Initiation and Execution. Cell *166*, 703–715.

Tepper, J.M., Wilson, C.J., and Koós, T. (2008). Feedforward and feedback inhibition in neostriatal GABAergic spiny neurons. Brain Res. Brain Res. Rev. *58*, 272–281.

Tunstall, M.J., Oorschot, D.E., Kean, A., and Wickens, J.R. (2002). Inhibitory interactions between spiny projection neurons in the rat striatum. J. Neurophysiol. *88*, 1263–1269.

Vaidya, M., Kording, K., Saleh, M., Takahashi, K., and Hatsopoulos, N.G. (2015). Neural coordination during reach-to-grasp. J. Neurophysiol. *114*, 1827–1836.

van den Berg, F.E., Swinnen, S.P., and Wenderoth, N. (2011). Excitability of the motor cortex ipsilateral to the moving body side depends on spatio-temporal task complexity and hemispheric specialization. PLoS ONE *6*, e17742.

Verstynen, T., Diedrichsen, J., Albert, N., Aparicio, P., and Ivry, R.B. (2005). Ipsilateral motor cortex activity during unimanual hand movements relates to task complexity. J. Neurophysiol. *93*, 1209–1222.

Whishaw, I.Q., Zeeb, F., Erickson, C., and McDonald, R.J. (2007). Neurotoxic lesions of the caudate-putamen on a reaching for food task in the rat: acute sensorimotor neglect and chronic qualitative motor impairment follow lateral lesions and improved success follows medial lesions. Neuroscience *146*, 86–97.

Wilson, C.J. (2007). GABAergic inhibition in the neostriatum. Prog. Brain Res. *160*, 91–110.

Wymbs, N.F., and Grafton, S.T. (2015). The Human Motor System Supports Sequence-Specific Representations over Multiple Training-Dependent Timescales. Cereb. Cortex *25*, 4213–4225.

Xu, T., Yu, X., Perlik, A.J., Tobin, W.F., Zweig, J.A., Tennant, K., Jones, T., and Zuo, Y. (2009). Rapid formation and selective stabilization of synapses for enduring motor memories. Nature *462*, 915–919.

Yin, H.H., and Knowlton, B.J. (2006). The role of the basal ganglia in habit formation. Nat. Rev. Neurosci. *7*, 464–476.

Yin, D., Valles, F.E., Fiandaca, M.S., Forsayeth, J., Larson, P., Starr, P., and Bankiewicz, K.S. (2009a). Striatal volume differences between non-human and human primates. J. Neurosci. Methods *176*, 200–205.

Yin, H.H., Mulcare, S.P., Hilário, M.R., Clouse, E., Holloway, T., Davis, M.I., Hansson, A.C., Lovinger, D.M., and Costa, R.M. (2009b). Dynamic reorganization of striatal circuits during the acquisition and consolidation of a skill. Nat. Neurosci. *12*, 333–341.

Yttri, E.A., and Dudman, J.T. (2016). Opponent and bidirectional control of movement velocity in the basal ganglia. Nature *533*, 402–406.

STAR★METHODS

KEY RESOURCE TABLE

REAGENT or RESOURCE	SOURCE	IDENTIFIER
Antibodies		
Anti-parvalbumin mouse monoclonal	Sigma-Aldrich	Cat# P3088, RRID: AB_477329
Anti-nitric-oxide-synthase goat polyclonal	Sigma-Aldrich	Cat# N7280, RRID: AB_260796
Anti-Leu-Enkephalin (NOC1) mouse monoclonal	Millipore	Cat# MAB350, RRID: AB_2268028
Substance P rabbit polyclonal	ImmunoStar	Cat# 20064, RRID: AB_572266
goat anti-rabbit	ImmunoStar	Cat# 20064, RRID: AB_572266
goat anti-mouse	Molecular Probes	Cat# A-21131, RRID: AB_141618
donkey anti-goat	Molecular Probes	Cat# A-11055, RRID: AB_2534102
Bacterial and virus strains		
pAAV-Ef1a-double.floxed- hChR2(H134R)-mCherry-WPRE-HGHpA	Gift from K. Deisseroth	Addgene viral prep # 20297-AAV1
pAAV-Ef1a-DIO eNpHR3.0-EYFP (AAV1)	Gradinaru et al., 2010	Addgene viral prep # 26966-AAV1
Chemicals, peptides, and recombinant proteins		
NBQX disodium salt hydrate	NBQX disodium salt hydrate	NBQX disodium salt hydrate
D(−)-APV, D-2-Amino-5-phosphonovaleric acid	Millipore Sigma	Cat# 79055-68-8
Gabazine (SR95531)– CAS 104104-50-9 - Calbiochem	Millipore Sigma	Cat# 104104-50-9
Lidocaine N-ethyl bromide (QX-314)	Millipore Sigma	Cat# 21306-56-9
Experimental models: cell lines		
Tg(Adora2a-Cre)	Transgene insertion KG139Gsat	Gensat RRID:MMRRC: 036158-UCD
Tg (Drd1-Cre)	Transgene insertion FK150Gsat	Gensat RRID:MMRRC: 036916-UCD

RESOURCE AVAILABILITY

Lead contact
For further information and requests for resources and reagents should be directed to and will be fulfilled by the Lead Contact, Gordon W. Arbuthnott (gordon@oist.jp).

Materials availability
This study did not generate new unique reagents.

Data and code availability
The published article includes all datasets generated or analyzed during this study.

EXPERIMENTAL MODEL AND SUBJECT DETAILS

Litters of mice bred at the OIST animal facility were kept in a room in a controlled environment (temperature: $21 \pm 1°$C; humidity 55%; light schedule 12/12 h with lights off at 7 p.m. after which behavioral training began) and were weaned at postnatal day 21. Weaned pups were housed in same- sex groups of 2–4. Standard rodent pellets and water were provided *ad libitum*, except when noted. We used mouse strains Adora2a-Cre and Drd1-Cre transgenic lines. For electrophysiological and behavioral experiments, only males, 32-40 days postnatal, were used. All procedures complied with guidelines, policies, and principles for experimental procedures, endorsed by the Society for Neuroscience and the government of Japan, and were supervised by the local Animal Care and Use Committee.

METHOD DETAILS

AAV expression and stereotaxic surgery

We used the following adeno-associated viruses (AAV): AAV1-dflox-hChR-2-mCherry, and AAV1- EF1a-DIO-eNpHR3-EYFP (Addgene). In aseptic conditions and under isoflurane anesthesia (IsoFlo Abbot, Ill), animals received a stereotaxic 0.2μL injection of either virus, at coordinates AP, 1.2mm; LM, 2.28; DV, 3.35 (Franklin and Paxinos, 2008).

6840855158115000After AAV injection, once the injection needle was slowly removed, a wireless stimulation device plus its optic fiber (250μm in diameter and 3.45mm long, TELEOpto BRC, UK) was inserted in the same place andrr fixed to the skull with dental cement (Super-Bond C&B, Sun Medical). Injections were unilateral for behavioral and bilateral for electrophysiological experiments. To allow viral expression and surgery recovery, animals were housed at least two weeks before any experimental procedures were performed.

The stimulation device triggered an LED of 470 nm (blue light) or 590 nm (yellow light) with intensity at the tip of 1.0 mW. Animals were habituated by carrying a mock receiver (12x18x7mm, 2g) plugged to the wireless stimulation system since the fourth day of training. During testing sessions, an infrared receiver with the same dimensions and weight replaced the mock unit. Continuous stimulation (10 s in average) was delivered when mice positioned themselves to start reaching and stopped when they grasped or missed the pellet. To deal with variations between groups, we normalized performance by comparing behaviors, before and after optogenetic manipulations in individual mice.

Single-pellet, reach-to-grasp task

We used a training chamber of the same dimensions and followed previously established procedures (Lopez-Huerta et al., 2016; Marques and Olsson, 2010). Briefly, after 4 days of recovery from surgery (W5- postnatal day 26) mice were deprived of food to ensure motivation. The schedule of food restriction for control and experimental animals provided enough nutrients to maintain approximately 90% of body weight during pre-training, and not less than 85% of body weight during training. As a reward, we used 20 mg dustless, chocolate-flavoured precision pellets (Bio-Serv, USA). During training and testing, mice received 20 pellets in a ≤ 10-min session daily. Three days prior to testing, mice were habituated to reward pellets scattered on the bottom of the cage once daily (0.4 g/animal/day). Daily, after training and testing, cage food was allowed. Mice were observed from the front of the cage. Shaping of the grasping response was performed in 10-min pre-training sessions for two days. The grasping response was made easier by gradually moving the pellet toward the indentation contralateral to the preferred paw (Miklyaeva et al., 1994). The first 10 reaching attempts were sufficient to identify the preferred paw. If a mouse used both paws, the one used more frequently (out of 10 reaches) was considered the preferred paw. Once the preferred paw was chosen, no mice changed paw use during the experiment. Two pre-training days were followed by 6-10 consecutive days of training, with daily sessions lasting until 20 pellets were successfully retrieved and eaten, or until a maximum of 10 min had elapsed. Starting on training day two, animals were trained to carry a mock receiver (12x18x7mm, 2g) plugged to the wireless stimulation system while performing the reaching task. Four days after, an infrared receiver with the same dimensions and weight replaced the training unit used for the wireless optogenetic stimulation during reaching. Performance was scored as reaching accuracy = (number of pellets retrieved/number of reaches) × 100 (Lopez-Huerta et al., 2016; Marques and Olsson, 2010).

Kinematic quantification of reaching

To analyze movement kinematics during reaching and grabbing, trained mice were placed in a reaching chamber with an angled mirror on the bottom (Figure 1). All reaching attempts were further analyzed in kinematics assessments. Behavior was recorded with one normal and two high-speed cameras (Azim et al., 2014). The two high-speed, high-resolution, monochrome cameras (MiCAM02-CMOS, Brainvision, Costa Mesa, CA) with 50mm f/1.4 manual iris and focus lenses (C-Mount) were placed at the front and the right or left-hand side of the chamber, depending on the preferred paw. Cameras were synchronized and videos were acquired using Brain Vision LLC analysis software. Cameras were set to 100 frames / second with a resolution of 376 × 252 pixels. White styrofoam walls were placed behind the sides and back of the chamber to reduce background and increase contrast.

We analyzed paw position using video recordings and the 2D manual tracking plugin of ImageJ. After coordinates were retrieved for each trial, further analysis was implemented in Origin (version 8.6, Microcal, Northampton, MA) and principal component analysis (PCA) and further neighbor search analysis were executed in MATLAB (Morris and Trivedi, 2011). Paw distance-to-pellet was calculated as the square root of $(x^{''} + y^{''})$. Velocity was calculated as the derivative of the distance, and acceleration as the derivative of the velocity. Mean position, distance, and velocity, were calculated by averaging the trials. The standard deviation is represented as the shaded region around the mean. Comparisons were made within the same mouse before and during experimental manipulation (20-30 reaches per condition). The percentage of errors was calculated by observing only the missed trials and quantifying the number of times the mouse changed the initial trajectory (initial error type I), changed the final trajectory (final error type II) or missed grasping the pellet (grasp error type III). Posture analysis utilized images from a panoramic view camera that captured the image of a mirror placed at a 45° angle under the training chamber. Different parameters of the stance were measured right before the preferred paw began to reach. We used FIJI to open images and to measure the angle between the mid-line of the body and the wall of the chamber, and the step and stride in hit and missed trials in all conditions (Figure 2G).

Slice preparation

Sagittal slices (250 μm) were obtained from AAV-injected animals 6-8 days after training and 2-weeks post-surgery, to allow viral expression. Control slices came from food-deprived littermates subjected to AAV-injection, but not training. Mice were anesthetized via isoflurane inhalation and perfused transcardially with cold saline containing (in mM): 124 choline chloride, 2.5 KCL, 2 MgCl2, 20 HEPES, 1.2 NaH2PO4-H2O, 1 CaCl2, 1 ascorbic acid, 3 pyruvate, and 10 glucose saturated with 95% O2 and 5% CO2, pH = 7.4, 298 mOsm/L. Slices were cut and transferred to regular artificial cerebral spinal fluid containing the following (in mM): 136 NaCl, 3.5 KCl, 1 MgCl2, 2.5 CaCl2, 26 NaHCO3, and 11 glucose saturated with 95% O2 and 5% CO2, where they remained for at least one hour before recording at room temperature (21–25°C).

Electrophysiological recordings

We performed whole-cell patch-clamp recordings with borosilicate glass pipettes (Harvard Apparatus 30-0057) heat-polished to obtain direct current resistances of 4–6 MΩ. Pipettes were filled with an internal solution containing (in mM): 115 KH_2PO_4, 2 MgCl2, 10 HEPES, 0.5 EGTA, 2 Na_2ATP, and 0.2 Na_2GTP or 72 KH_2PO_4, 36 KCl, 2 MgCl2, 10 HEPES, 1.1 EGTA, 2 Na_2ATP, 0.2 Na_2GTP, 5 QX- 314, and 0.5% biocytin (pH 7.2, 280mOsm) QX-314 prevented action potentials from occurring and allowed for stable voltage clamp recordings at depolarized membrane potentials. Recordings were made with a microelectrode amplifier using bridge and voltage clamp modes of operation (BVC-700A, Dagan Co, Minneapolis, MN). In some cases, conventional characterization of neurons was made in voltage- and current-clamp configurations. Access resistances were continuously monitored as < 20 MΩ. Experiments with changes over 20% were interrupted and terminated. We tested for residual current in about 80% of the recorded cells by adding glutamate and GABA receptor blockers and if we observed residual current we discarded the cell. Software designed in LabVIEW Environment (National Instruments) was used for data acquisition and data analysis employed Origin (version 8.6, Microcal, Northampton, MA). Because the spread of the virus varies from slice to slice, we took care that recorded cells were within the targeted region of the slice. Cells were within a 150 μm radius of the labeled area.

Stimulation

Synaptic events were evoked with light pulses of 500-900 μW intensity (488 nm wavelength) using an optic fiber, an LED driver, and a fiber-coupled LED light source (DC2100, OGKR2 Thorlabs, Newton, NJ). Single-pulse stimulation, 2-5 ms duration at a frequency of 0.1-0.5Hz, was controlled with a computer interface. Traces represent the average of near 5-min recordings (25-30 traces) for any given condition. When recordings were obtained from cells loaded with ChR2, we compensated for the voltage effects of the open channel by maintaining the cell at the reversal potential of the opsin (+20mV; Schneider et al., 2015).

Drugs

From Sigma-Aldrich, San Luis, MO. antagonists of glutamic acid receptors: AMPA receptor (NBQX, Cat# N183) and NMDA receptor APV (Cat# A8054). Antagonist of GABA receptors: GABA_A receptor gabazine (Cat# SR95531). For reversible blockade of fast sodium-dependent action potentials and voltage-dependent, non-inactivating sodium conductance: lidocaine N-ethyl bromide (Cat# QX- 314). All drugs were prepared freshly in stock solutions and added to media during experiments.

Histology

Mice were briefly perfused intracardially with phosphate buffer 0.01M (pH 7.4) followed by phosphate buffer containing 4% (weight/volume) paraformaldehyde and 14% saturated picric acid. Brains were post-fixed for at least 2 h and then cryoprotected in a 50/50 mixture of fixative and 20% sucrose in 0.01M phosphate buffered saline (PBS). Sections were cut at 60 μm on a sledge microtome with a freezing stage (Yamato electrofreeze, MC-802A), washed in PBS, and incubated in 20% normal goat serum (Vector Industries) for 1 h. Primary antibodies against parvalbumin, nitric oxide, enkephalin (NOC1) or Substance P were incubated overnight at 4°C and stained with secondary antibodies. At least 2 h were allowed for binding before rinsing in PBS. Sections were mounted on slides; was used to fix the coverslips. To inspect stained tissue, a confocal microscope (Carl Zeiss LSM780) was used and pictures were taken using ZEN software.

QUANTIFICATION AND STATISTICAL ANALYSIS

Given the complexity and number of experimental groups, sample size was chosen based on previous literature (Azim et al., 2014). A Shapiro-Wilk test was applied to the original data to assess normality of data distributions. Data withdrawn from a normal distribution was analyzed with a parametric, unpaired two-sample, two-tailed t test. Data withdrawn from a non-normal distribution were analyzed with a Mann-Whitney-Wilcoxon unpaired two-sample test, given the nature of data collection. Compared data had similar variance.

Data from behavioral experiments had a normal distribution and summary data are presented as means ± SEM. Statistical analysis was performed on original data and percentages of change are reported throughout the paper. Data from electrophysiological recordings did not manifest a normal distribution and summary data are presented as medians ± interquartile ranges (IQR) and

comparisons of original values of control versus ipsilateral, control versus contralateral, and ipsilateral versus contralateral were performed with unpaired non-parametric tests. No randomization was applied in any experiment. The experimenter was blinded for behavioral experiments for all conditions in the first stage of analysis (scoring, manual tracking of trajectories) and semi-blinded for the latest principal component analysis (PCA). For electrophysiological recordings, the experimenter was blinded for ipsilateral versus contralateral recordings at the moment of analysis (percentage of cells receiving connection and amplitude). There was no blinding in the analysis of IPSCs kinetics.